Materials Advances

ROYAL SOCIETY OF CHEMISTRY

PAPER

View Article Online
View Journal | View Issue

Cite this: *Mater. Adv.*, 2022, 3, 6853

para-Azaquinodimethane based quinoidal polymers for opto-electronic applications: impact of donor units on the opto-electronic properties†

Bharath Dyaga,[a] Sasikumar Mayarambakam,[ab] Olzhas A. Ibraikulov,[c] Nicolas Zimmermann,[c] Sadiara Fall,[c] Olivier Boyron,[d] Thomas Heiser,[c] Nicolas Leclerc,[e] Nicolas Berton[a] and Bruno Schmaltz*[a]

para-Azaquinodimethane (*p*-AQM) based quinoidal–donor (Q–D) alternating copolymers offer a unique opportunity to investigate the properties of quinoidal polymers. It was however reported that the band-gap increases with increasing number of donor aryl units, as a result of a weakening of the quinoidal character of the polymer backbone. To overcome this issue, herein two new polymers were designed and synthesized by incorporating fused donor (PAQM2T-TT) and vinylene linker (PAQM2T-TVT) units, following a strategy for enhancing the backbone planarity. The thiophene-containing polymers PAQM3T and PAQM4T were also synthesized for better understanding of the influence of structural variations. Thus, in comparison with PAQM3T and PAQM4T, PAQM2T-TT and PAQM2T-TVT exhibited a slight red shift in spite of having more extended donor units, which is consistent with enhanced planarity and quinoidal character as suggested by DFT calculations. It is also found that the different donor units have a limited impact on the HOMO energy level of the *p*-AQM copolymers. Transport properties are measured by field effect transistors, and the photovoltaic properties of these *p*-AQM based polymers are reported for the first time, as electron donor materials in inverted configuration devices. PAQM2T-TVT and PAQM2T-TT exhibit a planar structure leading to a hole mobility of respectively 3.8 × 10^{-2} cm^{-2} V s^{-1} and 1.7 × 10^{-2} cm^{-2} V s^{-1}. When combined with a fullerene acceptor in solar cells, the PAQM2T-TT polymer exhibited a highest PCE of 2.32%.

Received 2nd June 2022,
Accepted 8th July 2022

DOI: 10.1039/d2ma00628f

rsc.li/materials-advances

1. Introduction

Conjugated polymers (CPs) are widely used in organic electronics and opto-electronics due to their advantages, such as a tunable backbone, light weight, flexibility, low cost, and solution-processable fabrication.[1] After tremendous efforts from researchers, impressive hole mobilities of over 10 cm^2 V^{-1} s^{-1} and power conversion efficiencies (PCEs) of over 20% have been achieved in organic field effect transistors (OFETs) and organic solar cells (OSCs), respectively.[2,3] Among the strategies that have been developed to improve the performance of the organic semiconductors, the donor–acceptor (D–A) alternation is the most successful and adopted chemical approach, in which the bandgap of the semiconductor can be tuned by suitable donor and acceptor units.[4] However, an alternative approach based on bond-length alternation (BLA) minimization by using quinoidal units (Q) has shown to be promising as well.[5,6] Indeed, the quinoidal strategy offers new opportunities to tune the frontier energy levels and provides access to a new class of polymers with specific optical, electronic, and magnetic properties.[7] Therefore, in recent years, due to their unique advantages of rigid and coplanar structures and the delocalization of π-electrons, quinoidal small molecules and polymers have received increased attention in OFET and organic thermoelectric devices.[8] But their applications in OSCs is limited. Usually, quinoidal polymers show low bandgap with low-lying lowest unoccupied molecular orbital (LUMO) and high highest occupied molecular orbital (HOMO) energy levels due to a reduced BLA. However, the design of such molecules and polymers is limited by the high reactivity of the quinoidal structures that exhibit a diradical character.[9] Until now, few

[a] *Laboratoire de Physico-Chimie des Matériaux et des Electrolytes pour l'Energie (PCM2E), EA6299, Université de Tours, 37200 Tours, France. E-mail: bruno.schmaltz@univ-tours.fr*
[b] *Department of Chemistry, Indian Institute of Science Education and Research (IISER), Tirupati 517507, India*
[c] *Laboratoire ICube, Université de Strasbourg, CNRS UMR 7357, 67037 Strasbourg, France*
[d] *Université de Lyon, Université Lyon 1, CPE Lyon, CNRS UMR 5128, Laboratoire CP2M, Equipe PCM, 69100 Villeurbanne, France*
[e] *Institut de Chimie et Procédés pour l'Energie, l'Environnement et la Santé (ICPEES), Université de Strasbourg, CNRS UMR 7515, 67087 Strasbourg, France*

† Electronic supplementary information (ESI) available. See DOI: https://doi.org/10.1039/d2ma00628f

quinoidal building blocks such as benzodipyrrolidone (BDP),[10] naphthodipyrrolidone (NDP),[11] dipyrrolo[2,3-*b*:2′,3′-*e*]pyrazine-2,6(1*H*,5*H*)-dione (PzDP),[12] benzo[1,2-*b*:4,5-*b*′]-dithiophene-2,6-dione (BDTD),[13] thieno[3,2-*b*]-thiophene-2,5-dione (TTD),[13] 2,2′-bithiophene-5,5′-dione (BTD),[13] *para*-azaquinodimethane (*p*-AQM),[14] and isatin end-capped quinoid[8b] have been used in OFETs. Among all the above building blocks, only the benzodipyrrolidone (BDP) and dipyrrolo[2,3-*b*:2′,3′-*e*]pyrazine-2,6(1*H*,5*H*)-dione (PzDP), were used in solar cell applications. Wei Yue *et al.* reported a benzodipyrrolidone (BDP) and dithienopyrrole based D–A polymers with a PCE of 2.60% in solar cells.[15] Recently, Langheng Pan *et al.* reported a PzDP-based polymer as an acceptor in all-polymer solar cells, which showed a PCE of 2.37%.[16]

Among the above quinoidal units, *para*-azaquinodimethane (*p*-AQM) offers a unique opportunity to investigate properties of homogeneous full electron donor quinoidal-based conjugated polymers, as it is the only quinoidal building block that does not exhibit a strong electron acceptor character. *p*-AQM also presents advantages such as ease of synthesis, ease of backbone tuning, and rigid and coplanar conformation that can be enhanced by noncovalent intramolecular S···N interactions with neighbour thiophene units.[14,17–19] Noticeably, an unconventional trend was observed in quinoidal–donor (Q–D) *p*-AQM copolymers, where the bandgap increases upon increasing the number of thiophenes from two to four in the main chain.[14] This effect was attributed to the dilution of the quinoidal character of the alternated Q–D copolymer with the extension of the aromatic comonomer, similar to what is observed in D–A alternating copolymers.[20] Moreover, increasing the number of thiophene units may lead to increased torsional disorder along the polymer backbone, which limits the conjugation length. *p*-AQM containing semiconducting polymers usually exhibit low bandgap and near-infrared absorption, similar to those of diketopyrrolopyrrole (DPP) based polymers.[21] However, the bandgap in *p*-AQM containing polymers is higher compared to DPP polymers. This is due to the weak electron-accepting nature of the *p*-AQM unit. As mentioned above, in the literature, the bandgap of *p*-AQM polymers is increasing with the increasing number of aryl/thiophene units, whereas it decreases in DPP-based polymers.

To further investigate this trend in the bandgap, we designed and synthesized a series of Q–D copolymers based on *p*-AQM as a quinoidal unit (Q) that incorporate different thiophene donor comonomers (Scheme 1). The impact of the different thiophene donor comonomers on optical and electrochemical properties are systematically studied by using various techniques such as UV-visible absorption spectroscopy, cyclic voltammetry, photoelectron spectroscopy in the air (PESA), and density functional theory (DFT). All polymers exhibit a low bandgap (1.47–1.52 eV) and *p*-type charge transport properties. Among all, *p*-AQM polymer containing thiophene vinylene thiophene (PAQM2T-TVT) exhibited a planar structure and leads to a hole mobility of 3.8×10^{-2} cm^{-2} V s^{-1}. Moreover, when combined with fullerene acceptor, the *p*-AQM polymer containing thieno[3,2-*b*]thiophene (PAQM2T-TT) polymer exhibited a power conversion efficiency (PCE) of 2.32%.

2. Results and discussion

To investigate this bandgap trend, we chose the previously reported polymers PAQM3T and PAQM4T as reference polymers (Scheme 1). They consist of an alternating *p*-AQM unit with a donor segment three and four thiophenes long, respectively. First, we kept approximately the same thiophene segment length and altered the central two thiophenes by either the introduction of a fused thieno[3,2-*b*]thiophene (PAQM2T-TT), or insertion of a vinylene linker in the middle of the four thiophenes (PAQM2T-TVT). The two new resulting polymers were designed to reduce the conformational disorder and improve the coplanarity of the polymer backbone. The improved coplanarity may result in enhanced electron delocalization along the backbone as well as in the increased π–π intrachain and interchain interactions in the solid-state.[22–25] Long and branched dodecyl hexadecyl side chains were used on the periphery of *p*-AQM to improve the solubility of the resulting polymers. Given the reported odd–even effect on interchain interactions, the branching point was placed at the second carbon.[17]

2.1. Polymer synthesis

The synthetic strategies towards dibromo *p*-AQM monomer (**3**) and polymers are shown in Scheme 1. The detailed synthetic procedures and characterizations are described in the ESI.† The synthetic strategies for (*E*)-1,2-bis(5-bromothiophen-2-yl)ethene (**4**) and stannyl monomers (**5–7**) are shown in the ESI† (Scheme S1). The dibromo *p*-AQM monomer (**3**) has been synthesized by following a reported procedure.[14] Intermediate **2** was obtained by Knoevenagel condensation between 1,4-diacetyl-2,5-piperazinedione and 5-bromo-2-thiophenecarboxaldehyde. Alkylation was performed on **2** under mild basic conditions, and gave the dibromo *p*-AQM monomer (**3**) with good yield. All Q–D polymers were synthesized through Pd-catalyzed Stille cross-couplings of the dibromo *p*-AQM monomer (**3**) and the corresponding stannyl monomer units. The molecular weights of the Q–D polymers were evaluated using high temperature size exclusion chromatography (SEC) working at 150 °C (Fig. S1, ESI†). The number-average molecular weight ($\bar{M}_n$) of PAQM3T, PAQM4T, PAQM2T-TT, and PAQM2T-TVT, were measured to be 10.5, 10, 14, and 18.9 kg mol^{-1} with a dispersity ($Đ$) of 2.4, 2.5, 1.9, and 2.3, respectively (Table 1). Due to the to the shorter thiophene segment, PAQM3T is soluble at room temperature in common organic solvents like chloroform and chlorobenzene, while all other polymers are soluble in hot chlorobenzene (CB), and hot *o*-dichlorobenzene (*o*-DCB).

2.2. Optical and electrochemical properties

The UV-visible spectra of the *p*-AQM polymers were recorded in solution (*o*-DCB) as well as in thin films. All the results are depicted in Fig. 1, and the numerical data are summarized in Table 1. In the solution state, due to its higher solubility, PAQM3T exhibited a single-band absorption. All remaining polymers exhibited dual band absorption corresponding to 0–1 and 0–0 transitions, indicating the pre-aggregated state of polymers in solution.[17] This relative intensity of the 0–0 and 0–1 features has been shown to be related to the strength of the

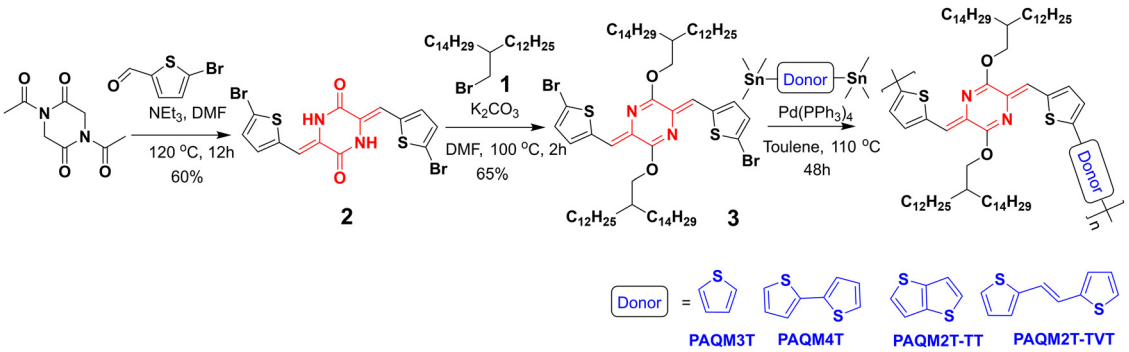

Scheme 1 Synthesis of dibromo *p*-AQM monomer and polymers.

Table 1 Solution and thin film UV-Vis absorption data of *p*-AQM series polymers

Polymer	$\bar{M}_n$ (kg mol^{-1})	$\bar{M}_w$ (kg mol^{-1})	$Đ$	$\lambda_{max}{}^a$ (nm)	$\lambda_{onset}{}^a$ (nm)	$E_g^{opt\,a}$ (eV)	$\lambda_{max}{}^b$ (nm)	$\lambda_{onset}{}^b$ (nm)	$E_g^{opt\,b}$ (eV)
PAQM3T	10.5	25.9	2.4	686	800	1.55	685, 758	835	1.48
PAQM4T	10.0	24.9	2.5	660, 729	807	1.53	655, 725	812	1.52
PAQM2T-TT	14.0	26.9	1.9	690, 765	826	1.50	690, 771	848	1.46
PAQM2T-TVT	18.9	43.1	2.3	675, 747	814	1.52	671, 745	830	1.49

[a] Measured in solution (*o*-DCB). [b] In the thin film state.

intermolecular coupling[26] and in some cases, to the type of polymer stack *i.e.*, segregated (0–0 band) *vs.* mixed (0–1 band).[27] Obviously the alkyl chain length does not impact the optical properties of PAQM4T, which is in good agreement with previous literature.[17] In the solution state, a significant bathochromic shift was observed for PAQM2T-TT and PAQM2T-TVT, compared to PAQM3T, and PAQM4T, due to π-extended fused thieno[3,2-*b*]thiophene in PAQM2T-TT and the longer conjugation length resulting from the vinylene group in PAQM2T-TVT. The absorption maxima of PAQM2T-TT and PAQM2T-TVT polymers are 765 and 747 nm, whereas the absorption maxima of PAQM3T, and PAQM4T, polymers are 682 and 729 nm, respectively. The optical band gap of all polymers was calculated from onset absorption in the solution state and all polymers exhibited moderate bandgap energy. In the solution state the optical bandgaps of all polymers followed the trend PAQM3T (1.55 eV) > PAQM4T (1.53 eV) > PAQM2T-TVT (1.52 eV) > PAQM2T-TT (1.50 eV).

In thin-films, all polymers exhibited dual band absorption. In the case of PAQM3T, the absorption spectra were broadened and a new shoulder peak appeared at 758 nm, which suggests a better solid-state order of the polymer backbone in the solid-state. Compared with PAQM3T, PAQM4T polymer absorption was blue-shifted, which is in agreement with previous literature.[14] Indeed, while increasing the number of aryl/thiophene units, the absorption spectrum was blue-shifted due to the BLA increase.[14] In the thin film-state, a red shift absorption was observed for PAM2T-TT, and it exhibits the maximum absorption in solution as well as in the solid-state compared to the other polymers. This shift is probably due to the higher rigidity of the TT unit, which is conducive to π-stacking self-assembly. Analysis of PAQM2T-TVT absorption spectra

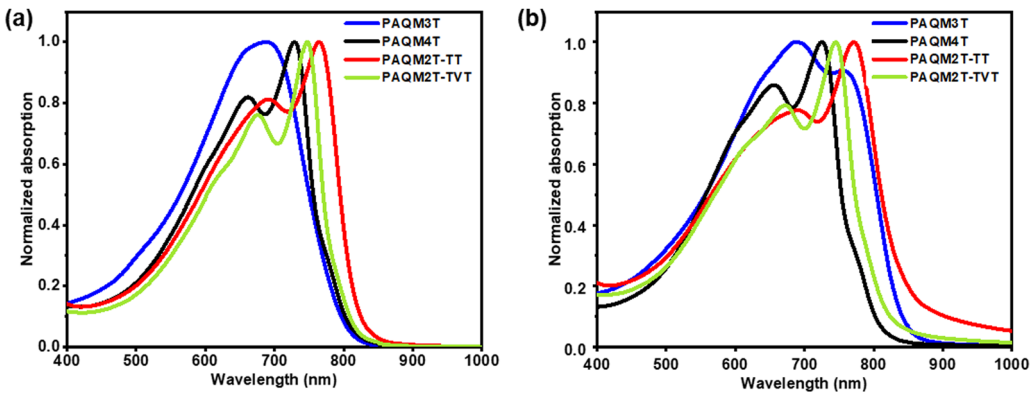

Fig. 1 (a) Absorption spectra of all polymers in solution (*o*-DCB), and (b) absorption spectra of all polymers in the thin film state.

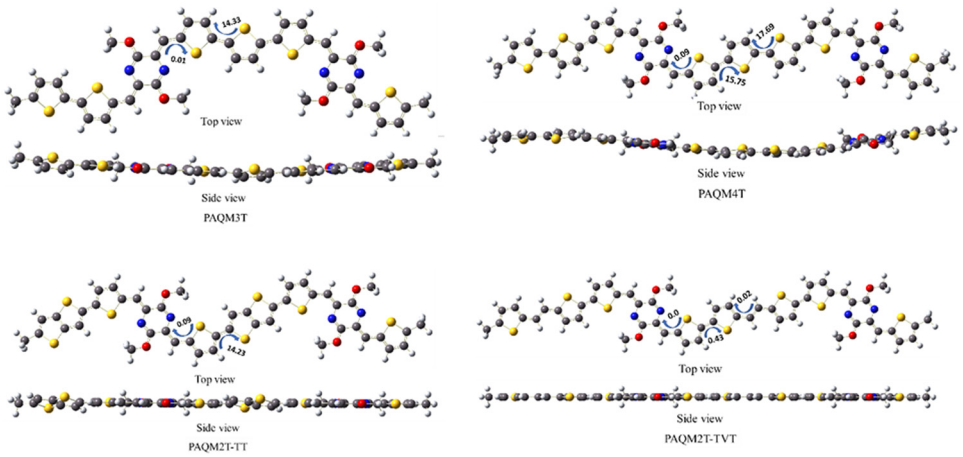

Fig. 2 Optimized geometries of the dimeric segments of *p*-AQM polymers, in which alkyl chains are substituted with methyl groups to simplify the calculation (top view and side view).

confirms that the dilution of the quinoid character and the twisting of the polymer chain are two equally important effects. Indeed, this PAQM2T-TVT polymer, which has the most extended electron-donor segment, nevertheless exhibits a

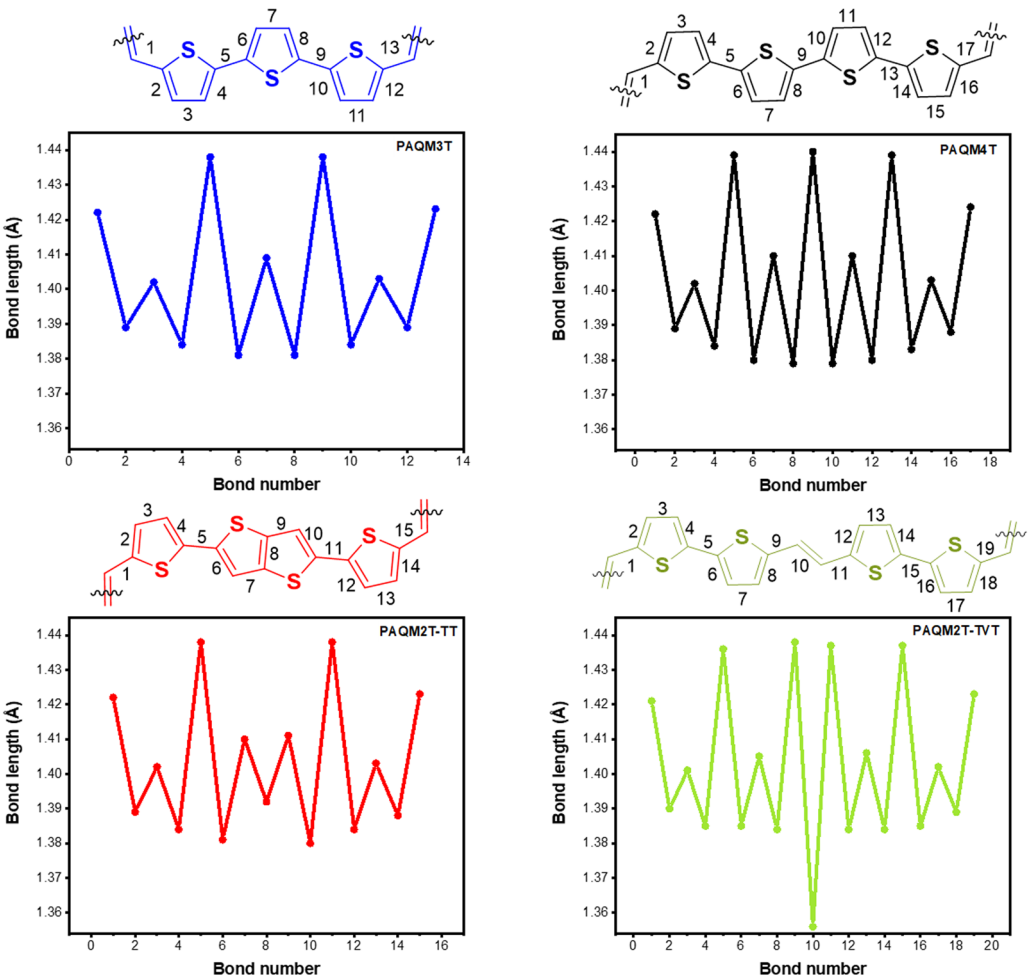

Fig. 3 Plots of carbon–carbon bond length for each respective bond number in the oligothiophene units in PAQM3T, PAQM4T, PAQM2T-TT and PAQM2T-TVT.

systematic red-shift of its absorption range compared to PAQM4T. This effect is clearly explained by density functional theory (DFT) calculations.

The DFT calculations are performed using Gaussian 9 at the B3LYP functionals and the 6-311g(d,p) basis set.[28] To simplify the calculations, two repeating units were considered for the polymer backbone, and long dodecyl hexadecyl side chains were replaced with methyl groups (Fig. 2). As expected, the insertion of vinylene linkage in-between two thiophene units leads to increased coplanarity. Thus, the dimer of the PAQM2T-TVT repeat unit adopts a highly planar conformation, as compared to the PAQM4T. PAQM2T-TT also adopts a highly planar configuration. Moreover, the insertion of vinylene linkage not only increases the coplanarity, but also alters the C=C, and C–C bond lengths on adjacent thiophenes, as indicated by bond length calculations. The C–C and C=C bond lengths of monomer segments of all polymers were calculated and are shown in Fig. 3. Noticeably, in agreement with previous reports PAQM4T exhibits longer C–C and shorter C=C bond lengths than PAQM3T on the central thiophene units, indicating a weaker quinoidal character. The C–C bond length at bond numbers 7 (1.405 Å) and 13 (1.406 Å) in PAQM2T-TVT were smaller compared to the C–C bond lengths at bond numbers 7 and 11 (1.410 Å) in PAQM4T. On the other hand, the C=C bond lengths at bond numbers 6 (1.385 Å) and 8 (1.384 Å) in PAQM2T-TVT were longer than the bond lengths at 6 (1.380 Å) and 8 (1.379 Å) in PAQM4T. Interestingly, the C–C bonds linking the *p*-AQM adjacent thiophene and vinylene adjacent thiophene (1.436 Å, bond numbers 5 and 15) were also slightly shorter in PAQM2T-TVT than the C–C bonds linking the *p*-AQM adjacent thiophene and bithiophene (1.439 Å, bond numbers 5 and 13) in PAQM4T. It clearly indicates that the introduction of a vinylene linkage leads to an increase in planarity, and decreases the BLA on adjacent thiophenes, hence improving an effective quinoidal conjugation in PAQM2T-TVT. In PAQM2T-TT, the central thieno[3,2-*b*]thiophene unit also contributes to the minimization of bond length alternation (BLA). The observed bathochromic shift in absorption can be ascribed to the BLA minimization resulting from the increased quinoidal character of PAQM2T-TVT and PAQM2T-TT.

Finally, the optical band gaps of all polymers were calculated from onset absorption in the thin film state. Due to the increased solid-state order in films, the optical band gap of PAQM3T was decreased from 1.55 eV to 1.48 eV. The optical bandgaps of the remaining polymers are slightly decreased compared to the solution state. The optical band gap of all polymers followed the trend in the thin film-state as PAQM4T (1.51 eV) > PAQM2T-TVT (1.49 eV) > PAQM3T (1.48 eV) > PAQM2T-TT (1.46 eV).

To investigate the energy levels of *p*-AQM polymers, we performed cyclic voltammetry (CV) measurements. The cyclic voltammograms of the four polymers are shown in Fig. 4, and the data are summarized in Table 2. The HOMO energy levels of all polymers are estimated to be −5.46, −5.48, −5.46, and −5.48 eV for PAQM3T, PAQM4T, PAQM2T-TT, and PAQM2T-TVT, respectively. The LUMO energy levels are calculated by adding the optical bandgap energies to the HOMO energy levels measured by CV.[29] The LUMO levels have been calculated to be −3.98, −3.96, −4.00, and −3.99 eV, for PAQM3T, PAQM4T, PAQM2T-TT, and PAQM2T-TVT, respectively. In a complementary way, photoelectron spectroscopy in the air (PESA) was also performed to estimate the HOMO energy levels. All the PESA spectra are depicted in the ESI† (Fig. S2), and data are summarized in Table 2. The ionization energies are −5.60, −5.61, −5.58, and −5.61 eV for PAQM3T, PAQM4T, PAQM2T-TT, and PAQM2T-TVT, respectively which is in good agreement with the trends given by CV and confirms that the impact of different thiophene comonomers on the polymer HOMO energy levels is negligible.

DFT calculations have been also used to probe the electron distribution in each frontier molecular orbital (Fig. 5). Thus, the HOMO electron distribution is evenly spread over the entire polymer backbone, and the LUMO delocalization is more reduced upon increasing the donor length. Indeed, the LUMO electron distribution is more evenly distributed over the entire

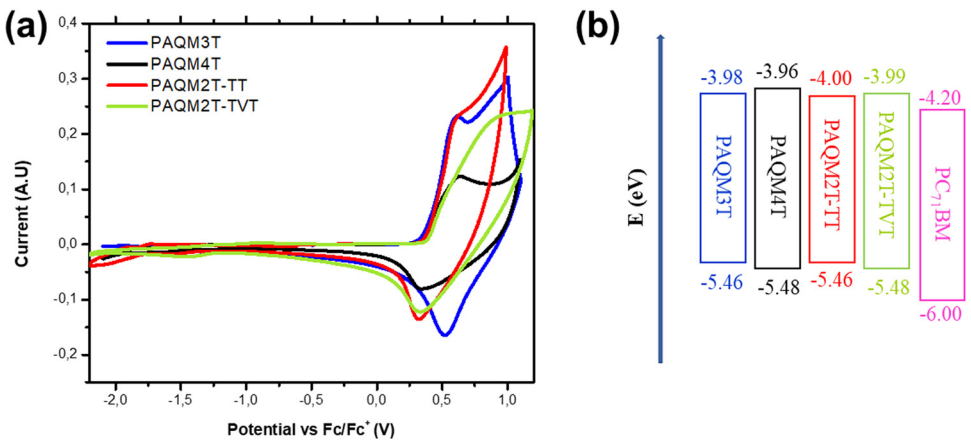

Fig. 4 (a) Cyclic voltammograms of *p*-AQM series of polymers where E_{ox} is the onset oxidation potential relative to the Fc/Fc^+ redox couple and (b) energy levels of the donor and acceptor.

Table 2 Electrochemical data of *p*-AQM series polymers

Polymer	E_{HOMO}[a] (eV)	E_{HOMO}[b] (eV)	E_{LUMO}[c] (eV)	E_{HOMO}[d] (eV)	E_{LUMO}[d] (eV)	T_d[e] (°C)
PAQM3T	−5.60	−5.46	−3.98	−4.66	−2.74	327
PAQM4T	−5.61	−5.48	−3.96	−4.68	−2.76	340
PAQM2T-TT	−5.58	−5.46	−4.00	−4.68	−2.78	367
PAQM2T-TVT	−5.61	−5.48	−3.99	−4.60	−2.81	372

[a] HOMO energy levels from PESA. [b] HOMO energy levels calculated from cyclic voltammetry using equation of $-(5.1 + E_{ox})$. [c] LUMO energy levels calculated from E_{HOMO} and λ_{onset} film. [d] Energy levels calculated from DFT. [e] Thermal decomposition temperature (T_d) corresponding to 5% weight loss.

backbone in PAQM3T than the other polymers, for which the LUMO is more localized on the the *p*-AQM moiety and less distributed on the donor moiety.

2.3. Thermal properties

The thermal properties of *p*-AQM series polymers were determined by thermo-gravimetric analysis (TGA) measurements and differential scanning calorimetry (DSC). All polymers are stable over 300 °C, indicating good thermal stability. The TGA and DSC plots are depicted in Fig. S3 (ESI†), and the corresponding data are summarized in Table 2. Thermal decomposition temperatures (T_d) corresponding to 5% weight loss are 328 °C, 340 °C, 367 °C, and 372 °C for PAQM3T, PAQM4T, PAQM2T-TT, and PAQM2T-TVT, respectively. DSC curves show that PAQM3T and PAQM4T polymers exhibit an exothermic phase transition at 43 °C and 45 °C, respectively, which can be ascribed to the melting of the alkyl side-chains.[30,31] PAQM3T also exhibited thermal transitions at 172 °C and 155 °C in heating and cooling cycles, indicating a semi-crystalline structure of the polymer. PAQM4T, PAQM2T-TT and PAQM2T-TVT do not exhibit any backbone-related thermal transition, which may indicate that the backbone is more rigid than that of PAQM3T. Moreover, the good thermal stability of *p*-AQM polymers indicates that they can be encapsulated without any structural change.

2.4. Field effect transistors

Charge transport properties are measured by bottom contact and bottom gate organic field-effect transistor (OFET) measurements (see the ESI† for details). All polymers exhibited p-type charge transport characteristics. Table 3 summarizes the average hole mobility for the four *p*-AQM-based polymers. Although the architectures of OFETs are not the most advanced ones, all polymers exhibited quite high hole mobilities, which highlights the potential of polymers based on quinoid units for charge transport applications, as reported in the literature.[14,17] The figures of the output and transfer characteristics of all polymers are outlined in Fig. 6. Among all the polymers, PAQM2T-TVT showed a hole mobility of 3.85×10^{-2} cm^{-2} $V\,s^{-1}$, which is one decade higher than previsouly reported vinylene linked polymer (PA2TV-BC2-C10C12).[17] The highest mobility of PAQM2T-TVT is attributed to the coplanar backbone resulting from the insertion of the vinylene double bond into the bithiophene, which leads to an increase in the intra- and inter-chain charge

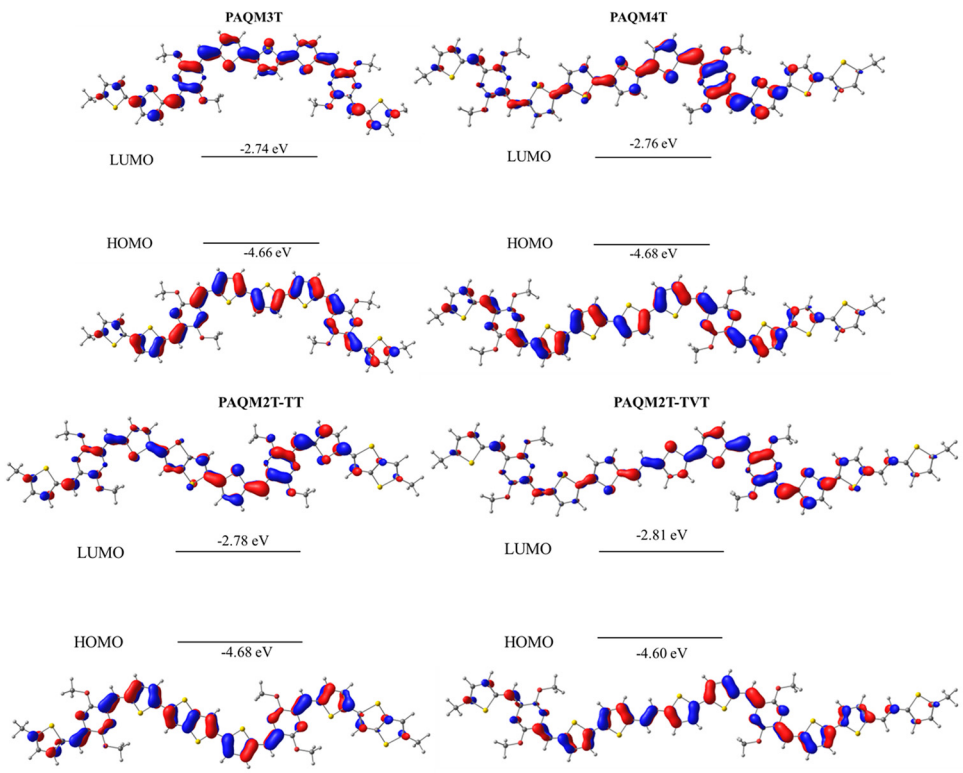

Fig. 5 Calculated molecular orbital distribution and energy levels of the dimeric segments of *p*-AQM polymers.

Table 3 OFET characteristics of *p*-AQM series polymers

Polymer	Film deposition	$\mu_h^{avg\,a}$ ($cm^2\ V^{-1}\ s^{-1}$)
PAQM3T	As cast	5.21×10^{-3}
PAQM4T	As cast	1.98×10^{-2}
PAQM2T-TT	As cast	1.74×10^{-2}
PAQM2T-TVT	As cast	3.85×10^{-2}

[a] Average mobility.

transfers in thin films.[23,24] PAQM2T-TT and PAQM4T showed almost similar hole mobilities of 1.74×10^{-2} and 1.98×10^{-2} $cm^{-2}\ V\ s^{-1}$, respectively and PAQM3T showed a hole mobility of 5.21×10^{-3} $cm^{-2}\ V\ s^{-1}$. The lower mobility of PAQM3T is not easy to explain. However, given the inversion of the relative intensities of the 0–0 and 0–1 bands for this specific polymer, compared to the others, with a possible maximum of mixed stacking, it can be assumed that the way in which the stacked backbones overlap is not favourable for efficient charge transport.

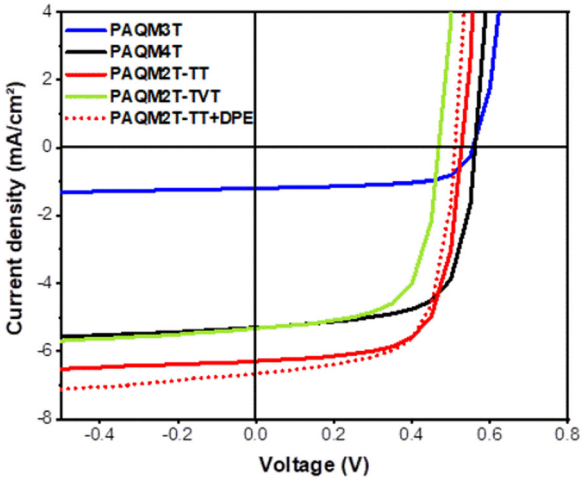

Fig. 7 Current density–voltage curves of *p*-AQM/$PC_{71}BM$ (1/1.5) (solid lines) and PAQM2T-TT + DPE/$PC_{71}BM$ (1/1.5) (dotted line) devices in the inverted configuration ITO/ZnO/Active layer/MoO_3/Ag.

2.5. OPV characterizations

The photovoltaic properties of these new *p*-AQM-based polymers, as electron donor materials, have been investigated in inverted device configuration: ITO/ZnO/Active layer/MoO_3/Ag (details can be found in the ESI†). The $PC_{71}BM$ fullerene derivative has been selected to act as an electron acceptor material. After careful optimization, we found the best D : A ratio to be 1 : 1.5 for all polymers (Fig. 7). A first optimization has been done under simple process conditions, using chlorobenzene as a solvent and warm solutions (around 80–90 °C) during the spin-coating. The photovoltaic parameters are summarized in Table 4.

A first trend is clearly emerging, with PAQM3T showing the lowest PCE, around 0.4%. In contrast, PAQM2T-TT has a higher

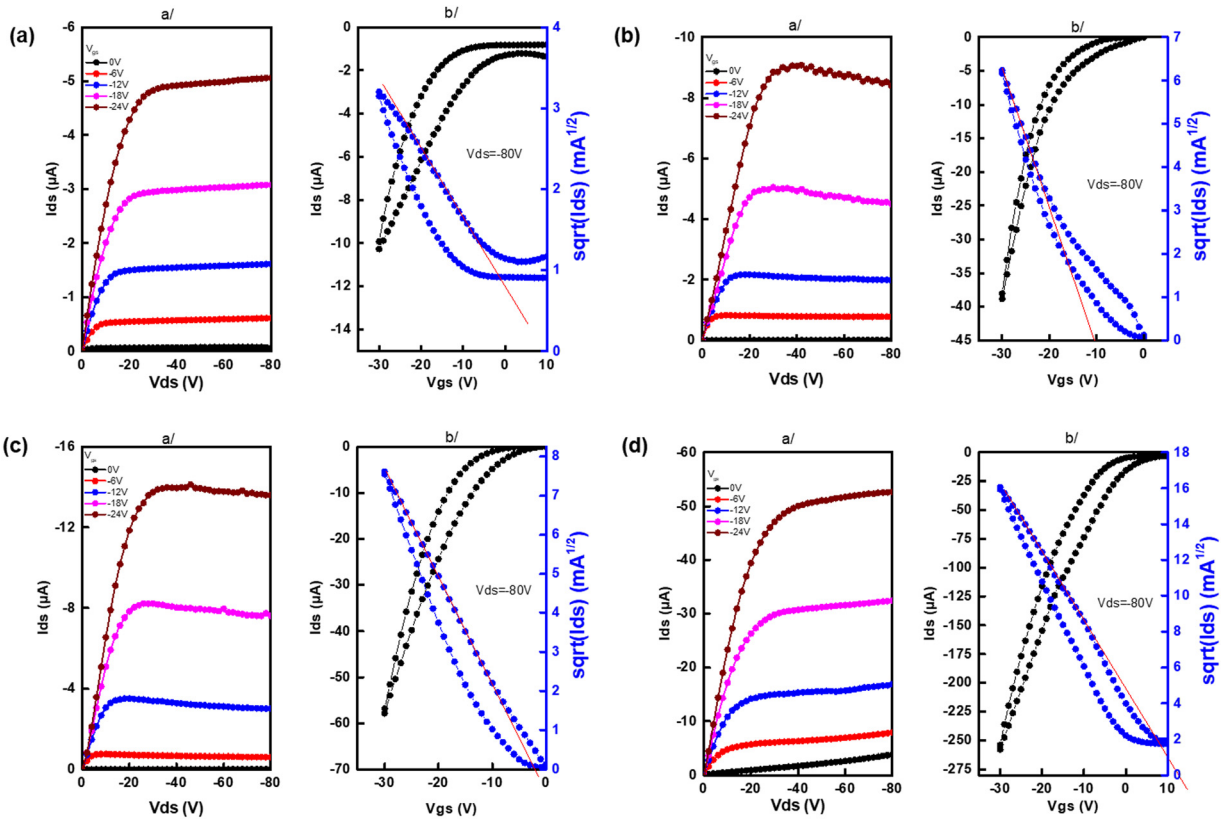

Fig. 6 a/Output and b/transfer characteristics of *p*-AQM polymer (a) PAQM3T (b) PAQM4T (c) PAQM2T-TT and (d) PAQM2T-TVT.

Table 4 OPV characteristics of *p*-AQM series polymers

Polymer	D–A ratio & solvent	V_{oc}	J_{sc}	FF	PCE
PAQM3T	1/1.5, CB	0.563 ± 0.05	1.1 ± 0.2	62.8 ± 2.6	0.39 ± 0.05
PAQM4T	1/1.5, CB	0.569 ± 0.003	5.08 ± 0.2	67.2 ± 0.6	1.95 ± 0.1
PAQM2T-TT	1/1.5, CB	0.527 ± 0.1	5.96 ± 0.4	65.5 ± 3.2	2.06 ± 0.2
PAQM2T-TVT	1/1.5, CB	0.474 ± 0.005	5.38 ± 0.2	63.9 ± 0.8	1.63 ± 0.05
PAQM2T-TT	1/1.5, CB, 3% vol DPE	0.517 ± 0.003	6.67 ± 0.2	67.4 ± 0.7	2.32 ± 0.08

PCE of almost 2.1%. PAQM2T-TVT and PAQM4T exhibit very close PCEs of 1.6 and 1.9%, respectively. The trend observed previously in OFET is consistent with the measured OPV performances. The poor performance of PAQM3T devices may be due to a lower charge extraction ability, while the other three polymers finally show similar hole mobilities and performances.

In order to give a chance to increase the performance, we tried to optimize the PAQM2T-TT-based active layer by playing with the additives. Finally, with 3%vol of diphenyl ether (DPE) as an additive, we slightly increased both the short-circuit current density and fill-factor, leading ultimately to a PCE slightly above 2.3% (Fig. 7 and Table 4). To the best of our knowledge, this study present the first report on the photovoltaic behavior of *p*-AQM-based polymers. Although moderate, such a PCE is ultimately in the same order of magnitude as those reported in the literature for other quinoid polymers.[15,16]

3. Conclusions

Here we reported two new polymers named PAQM2T-TT and PAQM2T-TVT. It is demonstrated that the quinoidal character of Q–D *p*-AQM-based copolymers can be enhanced *via* increased backbone planarity, thus paving the way toward low band gap quinoidal polymers with extended conjugation length. The newly synthesized polymers PAQM2T-TT and PAQM2T-TVT showed redshifted absorption and slightly reduced optical bandgaps compared with PAQM3T and PAQM4T polymers respectively. Cyclic voltammetry, photoelectron spectroscopy in air (PESA), and density functional theory (DFT) techniques confirmed that the impact of different thiophene donors on the *p*-AQM polymer HOMO energy level is limited. Both polymers exhibited a rigid backbone and exhibited moderate hole mobilities. Transport characteristics are measured for all polymers, and all exhibited p-type behaviour with a maximum hole mobility of 3.8×10^{-2} cm^{-2} V s^{-1}. The photovoltaic properties of *p*-AQM-based polymers were reported for the first time. The solar cells were constructed in the inverted device configuration and PAQM2T-TT exhibited the highest PCE of 2.32%.

Conflicts of interest

The authors declare no conflict of interest.

Acknowledgements

The authors gratefully acknowledge the Regional Council Centre-Val de Loire for support through the ETHERMO project. This work has also received support under the CERTeM 5.0 Program. B. S. and N. L. thank the Agence Nationale de la Recherche for financial support through the project ANR-17-CE05-0012S. B. S. would like to thank C-Valo for support through the SOLARPRINT project. M. S. thanks the Indian Institute of Science Education and Research (IISER)-Tirupati, Andhra Pradesh, Government of India for the computational studies.

References

1 (*a*) G. Yu, J. Gao, J. C. Hummelen, F. Wudl and A. J. Heeger, *Science*, 1995, **270**, 1789–1791; (*b*) M. Riede, D. Spoltore and K. Leo, *Adv. Energy Mater.*, 2021, **11**, 2002653; (*c*) H. Sirringhaus, *Adv. Mater.*, 2014, **26**, 1319–1335.
2 J. Yang, Z. Zhao, S. Wang, Y. Guo and Y. Liu, *Chem*, 2018, **4**, 2748–2785.
3 Z. Zheng, J. Wang, P. Bi, J. Ren, Y. Wang, Y. Yang, X. Liu, S. Zhang and J. Hou, *Joule*, 2021, **6**, 171–184.
4 P. M. Beaujuge and J. M. Fréchet, *J. Am. Chem. Soc.*, 2011, **133**, 20009–20029.
5 P. M. Burrezo, J. L. Zafra, J. T. López Navarrete and J. Casado, *Angew. Chem., Int. Ed.*, 2017, **56**, 2250–2259.
6 J. L. Bredas, *J. Chem. Phys.*, 1985, **82**, 3808–3811.
7 X. Ji and L. Fang, *Polym. Chem.*, 2021, **12**, 1347–1361.
8 (*a*) M. Yang, T. Du, X. Zhao, X. Huang, L. Pan, S. Pang, H. Tang, Z. Peng, L. Ye, Y. Deng and M. Sun, *Sci. China: Chem.*, 2021, **64**, 1219–1227; (*b*) X. Wei, W. Zhang and G. Yu, *Adv. Funct. Mater.*, 2021, **31**, 2010979; (*c*) Y. Sun, Y. Guo and Y. Liu, *Mater. Sci. Eng., R*, 2019, **136**, 13–26.
9 Z. Zeng, S. Lee, M. Son, K. Fukuda, P. M. Burrezo, X. Zhu, Q. Qi, R. W. Li, J. T. L. Navarrete, J. Ding and J. Casado, *J. Am. Chem. Soc.*, 2015, **137**, 8572–8583.
10 (*a*) W. Cui, J. Yuen and F. Wudl, *Macromolecules*, 2011, **44**, 7869–7873; (*b*) W. Cui and F. Wudl, *Macromolecules*, 2013, **46**, 7232–7238.
11 H. Zhang, J. M. Neudörfl and B. Tieke, *Polym. Chem.*, 2014, **5**, 3754–3757.
12 W. Hong, B. Sun, C. Guo, J. Yuen, Y. Li, S. Lu, C. Huang and A. Facchetti, *Chem. Commun.*, 2013, **49**, 484–486.
13 K. Kawabata, M. Saito, I. Osaka and K. Takimiya, *J. Am. Chem. Soc.*, 2016, **138**, 7725–7732.

14 X. Liu, B. He, C. L. Anderson, J. Kang, T. Chen, J. Chen, S. Feng, L. Zhang, M. A. Kolaczkowski, S. J. Teat and M. A. Brady, *J. Am. Chem. Soc.*, 2017, **139**, 8355–8363.
15 W. Yue, X. Huang, J. Yuan, W. Ma, F. C. Krebs and D. Yu, *J. Mater. Chem. A*, 2013, **1**, 10116–10119.
16 L. Pan, T. Zhan, J. Oh, Y. Zhang, H. Tang, M. Yang, M. Li, C. Yang, X. Liu, P. Cai and C. Duan, *Chem. – Eur. J.*, 2021, **27**, 13527–13533.
17 X. Liu, B. He, A. Garzón-Ruiz, A. Navarro, T. L. Chen, M. A. Kolaczkowski, S. Feng, L. Zhang, C. A. Anderson, J. Chen and Y. Liu, *Adv. Funct. Mater.*, 2018, **28**, 1801874.
18 L. Wang, X. Liu, X. Shi, C. L. Anderson, L. M. Klivansky, Y. Liu, Y. Wu, J. Chen, J. Yao and H. Fu, *J. Am. Chem. Soc.*, 2020, **142**, 17892–17896.
19 C. Liu, X. Liu, G. Zheng, X. Gong, C. Yang, H. Liu, L. Zhang, C. L. Anderson, B. He, L. Xie and R. Zheng, *J. Mater. Chem. A*, 2021, **9**, 23497–23505.
20 L. Biniek, C. L. Chochos, G. Hadziioannou, N. Leclerc, P. Lévêque and T. Heiser, *Macromol. Rapid Commun.*, 2010, **31**, 651–656.
21 (*a*) J. C. Bijleveld, A. P. Zoombelt, S. G. Mathijssen, M. M. Wienk, M. Turbiez, D. M. de Leeuw and R. A. Janssen, *J. Am. Chem. Soc.*, 2009, **131**(46), 16616–16617; (*b*) Y. Li, P. Sonar, S. P. Singh, M. S. Soh, M. Van Meurs and J. Tan, *J. Am. Chem. Soc.*, 2011, **133**(7), 2198–2204; (*c*) Y. Li, S. P. Singh and P. Sonar, *Adv. Mater.*, 2010, **22**(43), 4862–4866; (*d*) H. Chen, Y. Guo, G. Yu, Y. Zhao, J. Zhang, D. Gao, H. Liu,and and Y. Liu, *Adv. Mater.*, 2012, **24**(34), 4618–4622.
22 D. Gao, K. Tian, W. Zhang, J. Huang, Z. Chen, Z. Mao and G. Yu, *Polym. Chem.*, 2016, **7**, 4046–4053.
23 K. Takimiya, S. Shinamura, I. Osaka and E. Miyazaki, *Adv. Mater.*, 2011, **23**, 4347–4370.
24 W. Sun, Y. Chen, X. Liang, L. Tan, Z. Liu, Z. Cai, L. Dong and L. Wang, *New J. Chem.*, 2018, **42**, 15372–15378.
25 X. Liang, S. Gu, Z. Cai, W. Sun, L. Tan, L. Dong, L. Wang, Z. Liu, W. Chen and J. Li, *Chem. Commun.*, 2017, **53**, 8176–8179.
26 D. M. DeLongchamp, R. J. Kline, D. A. Fischer, L. J. Richter and M. F. Toney, *Adv. Mater.*, 2011, **23**, 319–337.
27 (*a*) M. Brinkmann, E. Gonthier, S. Bogen, K. Tremel, S. Ludwigs, M. Hufnagel and M. Sommer, *ACS Nano*, 2012, **6**(11), 10319–10326; (*b*) Y. Zhong, L. Biniek, N. Leclerc, S. Ferry and M. Brinkmann, *Macromolecules*, 2018, **51**, 4238–4249.
28 M. J. Frisch, G. W. Trucks, H. B. Schlegel, G. E. Scuseria, M. A. Robb, J. R. Cheeseman, G. Scalmani, V. Barone, B. Mennucci, G. A. Petersson, H. Nakatsuji, M. Caricato, X. Li, H. P. Hratchian, A. F. Izmaylov, J. Bloino, G. Zheng, J. L. Sonnenberg, M. Hada, M. Ehara, K. Toyota, R. Fukuda, J. Hasegawa, M. Ishida, T. Nakajima, Y. Honda, O. Kitao, H. Nakai, T. Vreven, J. A. Montgomery Jr., J. E. Peralta, F. Ogliaro, M. Bearpark, J. J. Heyd, E. Brothers, K. N. Kudin, V. N. Staroverov, T. Keith, R. Kobayashi, J. Normand, K. Raghavachari, A. Rendell, J. C. Burant, S. S. Iyengar, J. Tomasi, M. Cossi, N. Rega, J. M. Millam, M. Klene, J. E. Knox, J. B. Cross, V. Bakken, C. Adamo, J. Jaramillo, R. Gomperts, R. E. Stratmann, O. Yazyev, A. J. Austin, R. Cammi, C. Pomelli, J. W. Ochterski, R. L. Martin, K. Morokuma, V. G. Zakrzewski, G. A. Voth, P. Salvador, J. J. Dannenberg, S. Dapprich, A. D. Daniels, O. Farkas, J. B. Foresman, J. V. Ortiz, J. Cioslowski and D. J. Fox, Gaussian, Inc., Wallingford CT, 2013.
29 N. Berton, C. Ottone, V. Labet, R. de Bettignies, S. Bailly, A. Grand, C. Morell, S. Sadki and F. Chandezon, *Macromol. Chem. Phys.*, 2011, **212**, 2127–2141.
30 I. Osaka, R. Zhang, G. Sauve, D. M. Smilgies, T. Kowalewski and R. D. McCullough, *J. Am. Chem. Soc.*, 2009, **131**, 2521–2529.
31 Y. Wang and K. Takimiya, *Adv. Mater.*, 2020, **32**, 2002060.